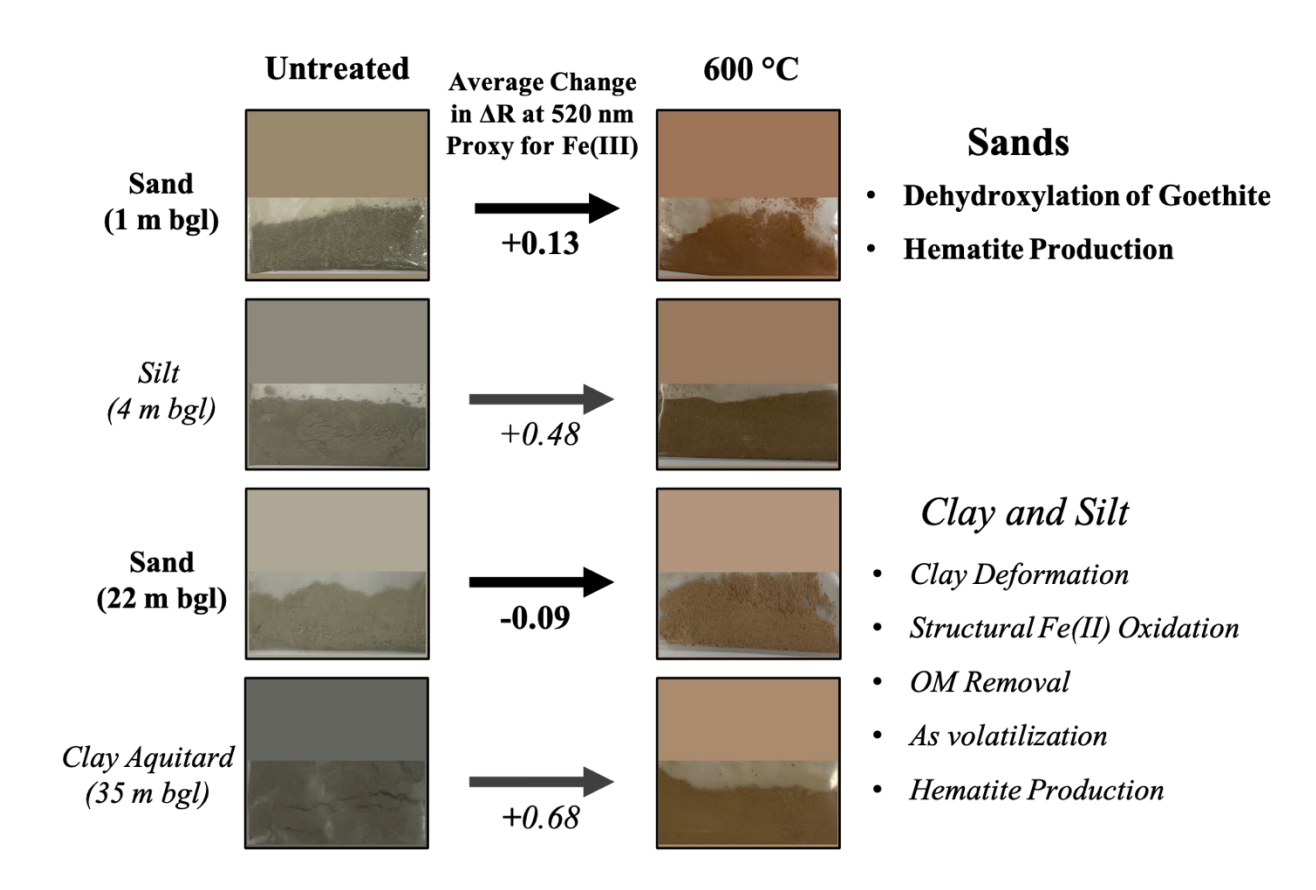
Mineralogical Association of Sedimentary Arsenic within a Contaminated Aquifer 1 **Determined through thermal Treatment and Spectroscopy** 2 3 4 Application of Thermal Treatment and Spectroscopic Techniques to Evaluate the Associations of Sedimentary Arsenic within a Contaminated Aquifer 5 6 Thomas S. Varner^{1*}, Harshad V. Kulkarni^{1,4*}, M Bayani Cardenas², Peter S.K. Knappett³, 7 8 Saugata Datta^{1*} 9 10 ¹Department of Earth and Planetary Sciences, University of Texas at San Antonio, San Antonio, TX, 78249, USA 11 ² Department of Geological Sciences, The University of Texas at Austin, TX 78712, USA 12 ³ Department of Geology and Geophysics, Texas A&M University, College Station, TX 77843, 13 USA 14 ⁴ School of Civil and Environmental Engineering, Indian Institute of Technology Mandi, 15 Himachal Pradesh, 175005, India. 16 17 Corresponding authors: Thomas S. Varner (tom.varner@my.utsa.edu), Harshad V. Kulkarni 18 (harshad.env@gmail.com / harshad@jitmandi.ac.in), Saugata Datta (saugata.datta@utsa.edu) 19 20 **Highlights** 21 22 1. The mineralogy of sediments from an As-contaminated aquifer and riverbank were spectroscopically characterized. 23 2. Elevated concentrations of As were associated with clay minerals containing Fe(II) and with 24 organic matter in fine-grained sediments. 25 3. As in sandy sediments was associated with Fe-hydroxide coatings and had lower 26 concentrations than finer grained sediment. 27 4. The sediment thermal treatment used provides a proxy for amount of organic matter and 28 structural Fe(II) in a sample. 29 30 Keywords: Arsenic; Diffuse Reflectance; Iron oxide; Meghna River; Clay mineral; 31 Colorimetry; Bangladesh 32

33 Graphical Abstract



Abstract

35

36

37

38

39

40

41

42

43

44

45

46

47

48

49

50

Sedimentary arsenic (As) in the shallow aquifers of Bangladesh is enriched in finer-grained deposits rich in organic matter, clays, and iron (Fe)-oxides. In Bangladesh, sediment color is a useful indicator for low As-aquifers. Orange sediment are usually high in Fe-oxides which As bounds to. Taking advantage of this color signal, spectroscopic measurements alongside thermal treatment have been extensively utilized for analyzing for Fe and clay minerals. This study uses Fourier transform infrared (FTIR) and diffuse reflectance (DR) measurements along with thermal treatment to evaluate the solid-phase associations of As from sediment along the Meghna River and its adjacent As contaminated aquifer in Bangladesh. Thermal treatment caused a deepening of reddish-brown hues in all samples, and the greatest change of color was observed in the fine-grain samples. Results revealed that clay minerals were composed primarily of phyllosilicates. The majority of Fe in sands was present as goethite; however, in the clay and silt samples, Fe was incorporated into the structure of clay minerals as Fe(II). Concentrations of As were highest in the fine-grain samples, after thermal treatment, the finer-grained samples showed higher removal of As (Avg = 40%) than sand samples (Avg = 20%). These findings indicate that significant proportions of solid-phase As may be regulated by OM and Fe(II)-bearing clay minerals.

1 Introduction

Geogenic arsenic (As) pollution in the shallow aquifers (< 60 m) of the Bengal basin threatens the health of millions who rely on the groundwater as their primary source of drinking water (Smith et al., 2000; Flanagan et al., 2012). Recent deposition of As-bearing sediments throughout the Holocene from the weathering of As-rich parent rocks along the Himalayan orogenic belt has been implicated as the primary source of As in the shallow aquifers of the Bengal basin (Smedley & Kinniburgh, 2002; Mukherjee et al., 2014; Chakraborty et al., 2015). The regional occurrence geogenic As and the heterogeneous distribution of As concentrations in the Holocene aquifers have complicated efforts to determine the exact nature of As in the sediments that is easily mobilized and dissolved into the groundwater.

The most plausible explanation and mechanism for the release of As from Fe minerals is the microbially mediated dissolution of Fe-oxide coatings on the surface of sand grains and clay minerals fueled by labile organic matter (Nickson et al., 1998; Nickson et al., 2000; Bhattacharya et al., 2001; McArthur et al., 2001; Islam et al., 2004; McArthur et al., 2004; Zheng et al., 2004; Hasan et al., 2007; Glodowska et al., 2020; Qiao et al., 2020; Vega et al., 2020). While the reductive dissolution of Fe-oxides may explain a relatively high proportion of the As released to solution, secondary minerals, such as Fe-oxides, are formed diagenetically in the sediment. Because of this, numerous other constituents have been cited as major hosts for As in the solid phase within the aquifer sediment including sulfides (Polizzotto et al., 2005; Polizzotto et al., 2006; Lowers et al., 2007), micaceous minerals and clays (Anawar et al., 2003; Hasan et al., 2007; Seddique et al., 2008; Masuda et al., 2012), and organic matter (Redman et al., 2002; Wang & Mulligan, 2006). Although the behavior of Fe-oxide minerals plays a prominent role in facilitating

the sequestration and mobilization of the dissolved As, the exact nature of the solid-phase As and its mobilizing pathways within the aquifer remains uncertain.

73

74

75

76

77

78

79

80

81

82

83

84

85

86

87

88

89

90

91

92

93

94

95

Much of the recent research has focused specifically on the association of As with Fe-oxides and reductive dissolution processes leading to the release of As from sediments. However, fewer studies have focused on the effects of organic matter and clay/phyllosilicate minerals on the solid phase partitioning of As. This is despite the fact that As has been reported to be consistently higher in organic-rich silt and clay sediments in the Bengal basin (Anawar et al., 2002; Smedley & Kinniburgh, 2002; McArthur et al., 2004; Nath et al., 2009; Varner et al., 2022). These fine-grained silt and clay sediments contain abundant organic matter with an affinity to strongly adsorb As (Deng & Dixon, 2002; Redman et al., 2002; Wang & Mulligan, 2006; Liu et al., 2011; Xue et al., 2019), and clay/phyllosilicate minerals that can adsorb or incorporate As in the mineral structure (Goldberg, 2002; Beaulieu & Savage, 2005; Charlet et al., 2007; Seddique et al., 2008; Masuda et al., 2012; Tabelin et al., 2017; Huyen et al., 2019). While it is true that OM in clays acts to mobilize As to the groundwater (Mihajlov et al., 2020), these OM rich layers may also retain large amounts of As. The associations between Fe, As, and OM in clays could arise from the affinity of Fe for both As and OM, allowing for the formation ternary As-Fe-OM complexes (Deng & Dixon, 2002; Sharma et al., 2010; Liu et al., 2011; Zhang et al., 2021). The association of both Fe and OM in the sediments may be exacerbated by the inclusion of Fe in the structure of clay minerals, as Fecontaining clay minerals are ubiquitous in fine-grained sediments and account for over 50% of the Fe mass in subsurface soils (Stucki, 2006; Stucki, 2011; Zhang et al., 2023). Furthermore, this structural Fe may exist as Fe(III) or become reduced by micro-organisms to form structural Fe(II) (Komadel et al., 1990; Komadel et al., 2006). The structural Fe(II) within clay minerals is typically highly reactive with its surroundings (Hofstetter et al., 2003; Neumann et al., 2008; Neumann et al., 2009; Huang et al., 2021). In spite of many observations on the associations between Fe, OM and clay minerals along with the occurrence of As, little is known about the exact control that these clay minerals exert on As availability and mobility in the Bengal basin.

The application of Fourier transform infrared spectroscopy (FTIR) is remarkably well suited for the detection of hydroxyl units and oxygen bonds in samples; it has therefore been extensively used for the identification of clay minerals as well as Fe-oxides and Fe-oxy(hydroxides) (Farmer, 1974a; Russell & Fraser, 1994; Frost et al., 1999; Frost et al., 2000; Ruan et al., 2002; Parikh et al., 2014; Madejová et al., 2017). Additionally, due to the variety of hues exhibited by Fe-oxides, the use of diffuse reflectance (DR) is a useful tool for the simple differentiation of individual Fe-oxide species present which reflect and absorb differently in the red and blue spectral regions (Torrent & Barrón, 2002). The combined use of FTIR and DR techniques provides a powerful framework for the identification of the most prominent Fe-oxide and clay minerals present in a bulk sediment sample.

The effects of temperature on the mineralogy of clays and Fe-oxides have been well documented as the composition and effects on these minerals from elevated temperatures are crucial for the optimal production of pigments, dyes, ceramics, and bricks (Edwards et al., 1998; Jordán et al., 2001; de Faria & Lopes, 2007; Manoharan et al., 2011). For example, the dehydroxylation of amorphous Fe and goethite begins at temperatures around 200°C and transforms to hematite above 300°C, whereas phyllosilicate minerals experience dehydration, oxidation, dehydroxylization, and decomposition as temperatures increase from 100°C to ~1000°C, although the range differs for various minerals (Murad & Wagner, 1996; Murad & Wagner, 1998).

The application of FTIR and DR to thermally treated (or heated) sediment samples may provide valuable insights in understanding the mineralogical associations present in the bulk sample. To our knowledge, the application of thermal treatment has not been used to analyze the sedimentary and mineralogical properties that determine the association of As in the sediments within contaminated aquifers. The visual and spectroscopic properties resulting from the thermal treatment of sediment from areas prone to high groundwater As may provide a simple and inexpensive technique to understand the behavior of sedimentary As and to quickly constrain relative aqueous As concentrations. We employed FTIR, DR, and X-Ray Fluorescence to determine the mineralogical response to the thermal treatment of sediments at 600°C in order to determine the importance of these sediments on As availability and mobility.

2 Methods

2.1 Study site

The detailed description of the study site and properties of the sediment samples are described elsewhere (Varner et al., 2022) (and Varner et al., 2023 in prep). Briefly, sediment samples from the riverbank and its adjacent aquifer were collected along the Meghna River in the Nayapara village (23.7°N, 90.7°E) within the Narayanganj district. The site consists of riverbank sands (0-3m bgl) composed of fine sand, a silt layer (3-7m bgl), a 29 m thick medium sand unit (7-36m bgl) that comprises the shallow aquifer, and a clay aquitard at 37m bgl. The samples are herein referred to by their abbreviated lithologies as RBS, SLT, AQS, and CLY, respectively. The riverbank sand (~1 m below ground level, bgl) was collected as pristine sediment cores using a direct push sediment probe (AMS inc., USA) (n = 2) and the SLT (6m bgl), AQS (23 m bgl), and CLY (37 m bgl) were collected as drill cuttings by the hand flapper method (n = 6) (Horneman et al., 2004). All samples used in this study were stored in Mylar Remel® bags with an O₂ absorbent pouch and

kept at -7°C until analysis. The site was chosen based reports of high As and Fe groundwater concentrations in the region (BGS&DPHE, 2001; van Geen et al., 2003; van Geen et al., 2014), and the previous identification of tidal activity and As enrichment in the riverbank sediments (Datta et al., 2009; Jung et al., 2012; Jung et al., 2015; Shuai et al., 2017; Berube et al., 2018).

2.2 Sample Preparation and Thermal Treatment

Two samples from each of the four lithologies (RBS, SLT, AQS, and CLY) were chosen for the analyses. The D10 grain size (10th percentile) of each of the samples was calculated following the particle size analysis results of the samples which is described in detail in Varner et al. (2022). The samples were dried in an N_2 environment and then powdered using an agate pestle and mortar. An aliquot of each sample was then placed in a furnace at 600 °C for three hours. In total, there were two untreated samples from each lithology and an aliquot of each sample underwent the thermal treatment for a total of 16 samples prepared for the analyses (n = 8 untreated, n = 8 thermally treated).

2.3 Fourier transform infrared measurements

A single beam Fourier transform infrared spectrophotometer (IRSpirit, Shimadzu Corporation, Japan) was used for the collection of the mid-infrared spectra of the sediment samples by the attenuated total reflectance (ATR) technique between the 4000-650 cm⁻¹ range. The ATR cell was equipped with a germanium-coated KBr beam splitter and a QATR-S diamond crystal attachment (45° angle of incidence). Data were collected as the average of 64 scans with a resolution of 4 cm⁻¹ and each resulting spectrum was automatically corrected for the ATR method by the instrument assuming a refractive index of 1.5 for the sample. A background reading was

collected between samples and subtracted from subsequent measurements. The resulting FTIR spectra were baseline corrected and smoothed in Spectragryph (v1.2.16.1).

2.4 Reflectance spectroscopy

Color is a conspicuous feature of Fe-oxy(hydr)oxides and diffuse reflectance (DR) spectroscopy techniques have been extensively used to quantify the color content for the characterization of iron-oxide mineral content in natural sediment samples (Strens & Wood, 1979; Morris et al., 1985; Torrent & Barrón, 2002). For this work, the DR spectrum of both the untreated and treated samples was collected using a CM-600d spectrophotometer (Minolta Corp.) and was recorded relative to a standard BaSO₄ white plate. The observer angle of the spectrophotometer was set to 10° with the exclusion of direct reflection specular components with an illuminant source of D65 corresponding to a color temperature of \sim 6,500 K. For DR measurements, the sample was placed in a cut paper cup (diameter = 2.5 cm) and was smoothed and covered with clear polyethylene wrap to provide a planar surface for measurements. Each sample data spectrum is the automated average of 5 readings, the white standard plate was measured before the collection of each sample spectrum. The first transform derivative of the reflectance spectra (Δ R) was then obtained by taking the difference of % reflectance of the two adjacent 10 nm wavelength measurements for a given point.

2.5 X-Ray Fluorescence

The elemental concentrations of As were measured by X-Ray fluorescence (XRF) in each of the 16 samples using a Niton XL3t 500 GOLDD handheld XRF spectrometer (Thermo Scientific, Cat no. XL3TGOLDDPLUS). The analysis settings were employed for the optimum measurement of heavy elements in soils with a SiO₂ matrix. To collect the data, the analyzer was placed directly

on each sample and analyzed for a total of 120 seconds (60 s main filter, 30 s low filter, and 30 s light filter) at a maximum voltage of 40 kV. The XRF measurements for As of standard reference materials (NIST 2709a, NIST 2780, CCRMP Till-4) yielded an average relative percent difference of 6.4 % from the certified values, well within the accepted range of error (± 20 %) for the instrument. A conservative method detection limit (MDL) was determined as three times the instrument's 2σ measurement error measured in samples with none or trace amounts of each analyte, as defined by the EPA SW-846 method 2600 definition of detection limits for XRF.

3 Results

3.1 FTIR

The FTIR results of the untreated samples between 1400 and 400 cm⁻¹ reveal spectra with 5 main peaks centered at ~1030, ~790, ~690, ~530 cm⁻¹, and ~470 cm⁻¹. The highest absorbance for all peaks was recorded in the clay and was lower for all peaks in the sand samples (Fig. 1a). The vibrational assignment of the peaks found in this study are presented in Table 1. Briefly, the assignment of the peaks at ~1030, ~790, ~690, ~530 cm⁻¹, and ~470 cm⁻¹ are primarily attributed to antisymmetric Si-O-Si stretching, symmetric Si-O-Si stretching, perpendicular Si-O stretching, Si-O-Al^{VI} bending, and Si-O-Si bending, respectively (Farmer, 1974b; Madejová et al., 2017). Smaller secondary peaks may provide diagnostic information and occur in the FTIR spectra at ~915 cm⁻¹ as a shoulder, a broad band between 800 and 740 cm⁻¹, at 435 cm⁻¹ and are attributed primarily to $\delta(Al_2OH)$ deformation, Fe(III)Mg-OH bending or Al^{IV}-O-Si in-plane vibration, and Si-O-Si bending, respectively (Farmer, 1974b; Madejová et al., 2017).

The thermal treatment resulted in a considerable decrease in the intensity of each sample spectra along all wavelengths (Fig. 1b). The alterations caused by thermal treatment can be easily observed in the difference between the untreated sample spectra and the spectra of the thermally

treated samples (Fig. 1c). The greatest amount of change caused by the thermal treatment were observed in the peaks located at ~1022, 912, between 800 and 750, 689, 530, and 464 cm⁻¹, associated mostly with various Si-O and Al-O vibrations. Thermal alterations were most noticeable in the clay and silt samples and produced minimal changes in the sand samples as seen by the relatively flat absorbance in the differential FTIR spectra (Fig. 1c, Table 1). The spectra of the treated samples retained a broad peak at ~1030 cm⁻¹, a small peak between 800 and 700 cm⁻¹ and produced a broad sloping peak at 460 cm⁻¹ in lieu of the two distinct peaks in the original sample

Table 1. Assignment of the vibrational peaks in the FTIR spectra between 1400 and 400 cm⁻¹. Data for the table was constructed from Farmer (1974b) and Madejová et al. (2017) unless stated otherwise.

Peak (cm ¹)		D	Mineral Associations		
This Study	Vibration Assignment	Reported Peak Center (cm ¹)			
1029	Asym. Si-O-Si Stretching	1000-1040	Kaolinite, illite, smectite, muscovite		
940-890	$\delta(Al_2OH)$	915-935	Kaolinite, illite, muscovite		
	δ-OH deformation	888-916 a, b, c, d	goethite, hydrohematite		
800-740	Sym. Si-O-Si stretching	798 and 780	Quartz doublet		
	γ–OH deformation	795 a, b, c, d	Goethite		
	Fe ³⁺ Mg-OH bending	765	Smectite		
	Al ^{IV} -O-Si in-plane	756	Illite		
691	Perpendicular Si-O	695	Kaolinite, quartz		
534	Si-O-Al ^{VI} bending	540-524	Kaolinite, smectite, illite		
	Fe-O	530-536 ^{a, b}	Hematite, goethite		
467	Si-O-Si bending	470	Kaolinite, smectite, illite, muscovite		
	Fe-O	452-460 a, b, c	Hematite, goethite		
435	Si-O-Si bending	428-443	Smectite, illite, muscovite		

^a Ruan et al. (2002)

207

208

209

210

211

212

213

214 spectra at 534 cm⁻¹ and 467 cm⁻¹ (Fig. 1a, b).

^b Chen et al. (2021)

^c Prasad et al. (2006)

d Margenot et al. (2016)

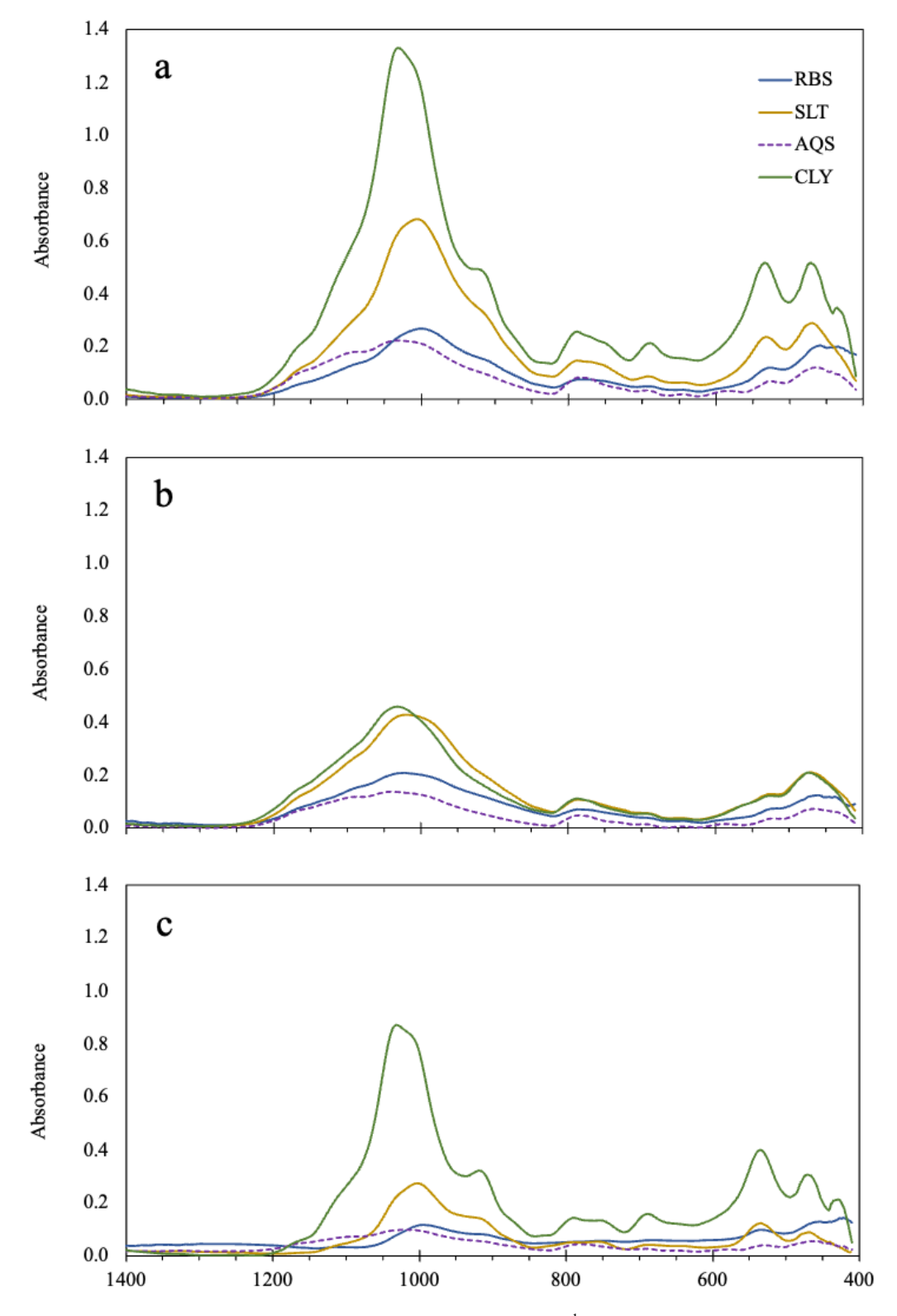


Figure 1. (a) FTIR spectra between 1400 and 400 cm⁻¹ of the untreated sediment from representative lithology samples; (b) FTIR spectra of the sediment subjected to thermal treatment at 600°C; (c) The difference between the untreated and thermally treated FTIR spectra of the same representative samples to show the locations of absorbance changes from the thermal treatment.

3.2 Diffuse Reflectance measurements

Consistent with previous studies, the reflectance spectrum of sediments with deeper brown and orange hues is elevated in the 550 to 700 nm range than that of grey sediment which typically displays a flatter reflectance spectrum in this range (Fig. 2a) (Horneman et al., 2004; Lugassi et al., 2014). In the fresh, untreated samples, the AQS samples displayed the highest values with an apparent slope in the DR spectra throughout the 400 to 700 nm range as opposed to the RBS, SLT, and CLY which contained similar values each other (Fig. 2a). Thermal treatment of the samples at 600°C caused an increase in brown-orange hues in all samples as reflected in the increased slope of the DR spectra (Fig. 2a).

The ΔR is highly reproducible and provides indicative information on the mineralogy of Feoxides. For example, Horneman et al. (2004) found that the ΔR at 520 nm is correlated to the Fe(II)/Fe(Total) content in the sediment, whereas other authors have noted that the first derivative spectra is a sensitive indicator for hematite and goethite with peaks occurring between 555 and 575 for hematite and two peaks between 420-430 and 480 to 530 for goethite (Balsam & Damuth, 2000; Arimoto et al., 2002; Wu et al., 2016; Cao et al., 2022). The ΔR spectra of the untreated and thermally treated sediment samples show contrasting results (Fig. 2b). The ΔR at 520 nm of the untreated samples was typically lower than the ΔR at 520 nm of the thermally treated counterparts (Table 1), indicating an increase in the proportions of Fe-oxides. In the SLT and CLY samples, the ΔR at 520 nm increased an average of 53% following the thermal treatment, whereas that of the sand samples increased only an average of 1% from the same treatment. All untreated samples lack the hematite peak centered around 560 nm, rather, peaks at 420 and 500 nm indicate the presence of goethite in the samples, specifically in the RBS and AQS. The thermal treatment caused the goethite peaks at 420 and 500 nm to diminish and produced a large peak between 550

and 560 nm, indicating the formation of hematite (Fig. 1b). Furthermore, a new peak at 450 nm formed in the thermally treated samples which is a product of the thermal transformation of goethite to hematite in the DR spectra (Lugassi et al., 2014). The hematite peak of the AQS and CLY samples contained a lower intensity and was centered at 550 nm whereas the that of the RBS and AQS contained a higher intensity and was centered at 560 nm.

Table 2. Results showing the first transform derivative of the reflectance at 520 nm and the measured concentrations

of As and Fe in the samples before and after the thermal treatment. Results in parentheses are below the MDL.

	As (mg/kg)		Fe (g/kg)		ΔR at 520 nm	
	Untreated	Treated	Untreated	Treated	Untreated	Treated
RBS-1	5.42	4.42	30.04	24.61	1.02	1.25
RBS-2	6.61	4.80	28.84	26.69	0.72	0.75
SLT-1	8.13	6.71	40.08	32.29	0.45	0.89
SLT-2	6.39	3.85	34.03	29.47	0.44	0.96
AQS-1	(1.33)	(1.16)	5.36	4.46	1.01	1.02
AQS-2	(1.33)	(1.06)	6.57	5.31	1.2	1.02
CLY-1	11.49	4.66	37.18	14.28	0.6	1.25
CLY-2	11.22	6.25	36.54	24.71	0.52	1.22

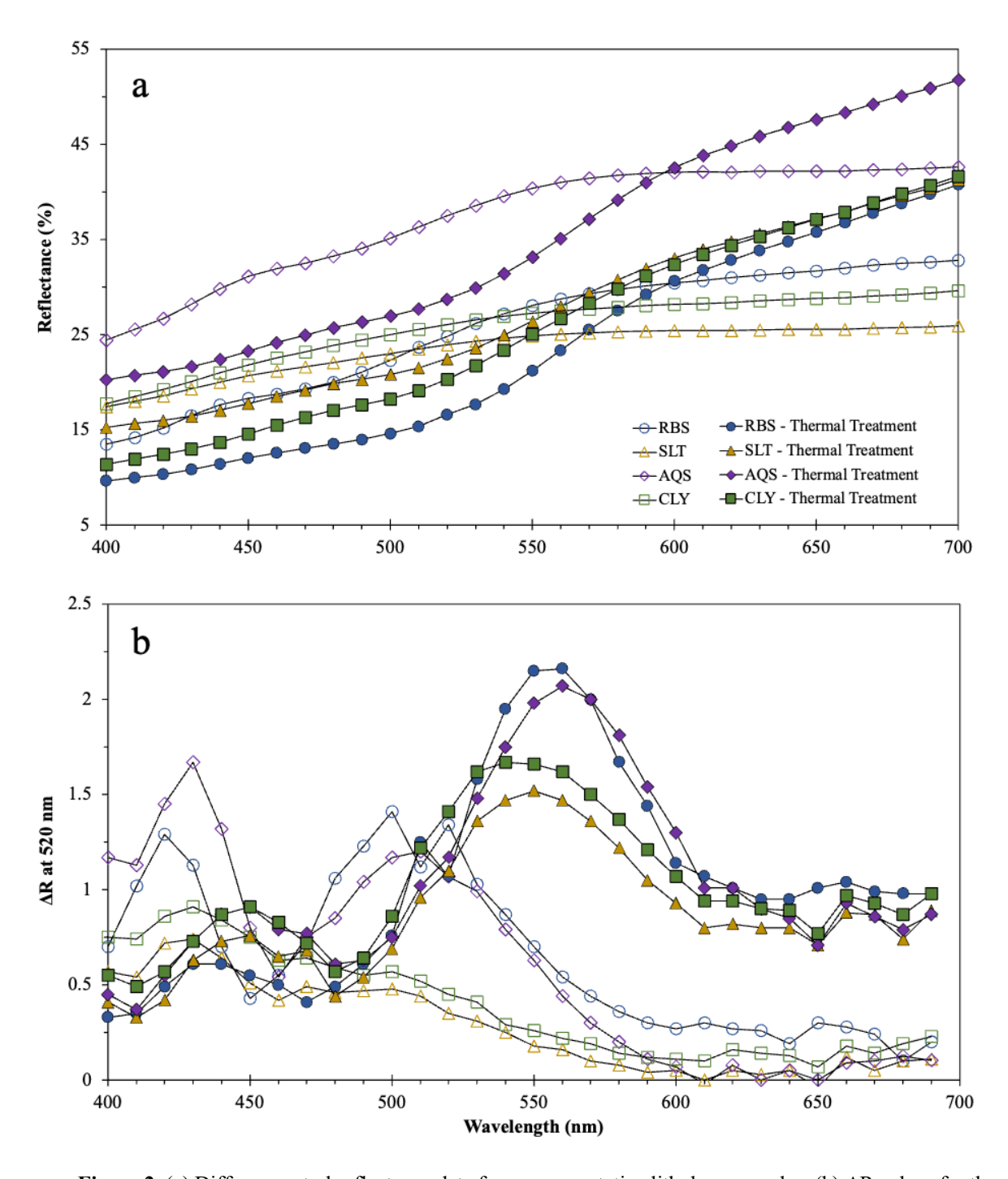


Figure 2. (a) Diffuse spectral reflectance data from representative lithology samples; (b) ΔR values for the same representative samples from each lithology. The open symbols represent the untreated samples, and the filled symbols represent the thermally treated samples.

3.3 Elemental concentrations

Initial concentrations of both As and Fe were higher in all samples before thermal treatment (Table 2). The concentrations of As in the AQS samples were above the instrument detection limit of 1.1 mg/kg. However all measurements of AQS samples were lower than the MDL of 3.5 mg/kg. The initial concentrations of As in the RBS, SLT, AQS, and CLY (6.0, 2.3, <1.3, 11.4 mg/kg, respectively) were comparable to values previously reported for similar sediments at the site (Varner et al., 2022). The concentrations of As decreased after the thermal treatment by an average of 1.4, 2.3, 1.1, and 6.25 mg/kg for RBS, SLT, AQS, and CLY, respectively. The concentrations of Fe in the RBS, SLT, AQS, and CLY (29, 37, 6, and 37 g/kg, respectively) were higher than the measurements following thermal treatment (26, 31, 5, and 20 g/kg, respectively). In general, the concentrations of the untreated sediment are within the ranges of previously reported sedimentary concentrations using XRF along the Meghna Riverbank and adjacent floodplain aquifer (Anawar et al., 2002; Jung et al., 2015; Berube et al., 2018).

4 Discussion

4.1 Spectral and IR changes in clay mineralogy in response to thermal treatment

The FTIR spectra is often dominated by the most abundant vibrational frequencies in the spectra. Given that Al, Fe, and Si make up most of the elemental composition of the RBS, SLT, AQS, and CLY sediments (average = 88%, 84%, 92%, and 85%, respectively) (Varner et al., 2022), the FTIR spectra are observed in the context of these elemental concentrations. Furthermore, clay minerals are especially sensitive to IR spectroscopy since the predominant vibrations in the near infrared range (hydroxyl groups and the Si-O network) are enriched in clay

minerals (i.e., O–H, Si–O, Al–O, Fe–O and Mg-O bonds) (Frost et al., 1999; Frost et al., 2000; Ruan et al., 2002).

267

268

269

270

271

272

273

274

275

276

277

278

279

280

281

282

283

284

285

286

287

288

289

The FTIR spectra of the untreated sediment displayed peaks that are characteristic of 1:1 and 2:1 layered clay minerals (Farmer, 1974b; Komadel et al., 2006; Madejová et al., 2017). A diagnostic peak of clay minerals occurs from the strong Si-O-Si vibrations centered at ~1030 cm⁻¹ 1, the shape of this dominant peak may provide further distinction of the clay minerals present. For example, the extensive substitution within the sheets of 2:1 clay minerals (i.e., smectite, illite, muscovite) results in a broadening of this peak centered at 1030 cm⁻¹ which may obscure the two distinct Si-O vibrations produced by kaolinite at ~1035 cm⁻¹ and 1010 cm⁻¹ (Farmer, 1974b; Madejová et al., 2017). However, the occurrence of kaolinite can be confirmed by the peak at 691 cm⁻¹ attributed to the perpendicular Si-O vibration in the mineral lattice of kaolinite (in conjunction with an absorbance band ~755 cm⁻¹). On the other hand, the presence of smectites is inferred by a diagnostic band near 430 cm⁻¹ attributed to the Si-O-Si bending bands, whereas a band near 756 cm⁻¹ resulting from Al-O-Si in-plane vibration is diagnostic of the structure of illite minerals (Farmer, 1974b). Furthermore, the untreated FTIR spectra of the samples, specifically in CLY, showed a slight shoulder between ~940 and 915 cm⁻¹ which is often attributed to the OH bending of inner-surface OH groups of Al₂OH in kaolin minerals and the δ((Fe)Al₂OH) bending of substituted illites and smectites (Madejová et al., 2017). Although not quantified, the FTIR spectra indicates that together, illite, smectite, and kaolinite contribute to the clay mineral assemblages found in the riverbank and aquifer sediments.

This finding is further supported by the chemical index of alteration (CIA) of the bulk samples (Fig. 3). As defined by Nesbitt and Young (1982), the CIA provides the extent of weathering of plagioclase and K-feldspar to their aluminous weathering products (i.e., clay minerals) and is

determined as CIA = [Al₂O₃ / Al₂O₃ + CaO* + Na₂ + K₂O)] * 100, where the elements are represented by their molecular proportions and CaO* represents CaO in the silicate fractions. Using the elemental concentrations presented in Varner et al. (2022) of the same samples, the bulk sediment CIA values of the RBS, SLT, AQS, and CLY samples averaged 65, 69, 61, and 78%, respectively. These values indicate only a moderate amount of chemical weathering, consistent with the rapid erosion and recent deposition of the Holocene aquifers of Bangladesh. Here, the CIA is determined from the bulk elemental composition of the sediments, rather than only the clay fractions. However, based on the FTIR and CIA results, the predominant clay minerals in these sediments are inferred to be illite and smecitite, and, to a lesser extent, kaolinite (Fig. 3). This finding is similar to previous studies which have used X-Ray diffraction analysis to identify the occurrence of feldspars, and clay minerals such as kaolinite, micas, smectite, and illite in aquifer sediment along the Meghna River (Seddique et al., 2008; Berube et al., 2018) and a large contribution of illite, smectite, chlorite, and kaolinite to the overall sediment load in the Bengal basin rivers (Allison et al., 2003; Khan et al., 2019; Ayers et al., 2020).

The thermal treatment of the samples at 600°C caused noticeable changes to the spectroscopic properties of the sediment. The most notable change in the FTIR spectra was the overall diminishing of the peaks located at ~1022, 912, between 800 and 750, 689, 530, and 464 cm⁻¹ (Fig. 2c). These peaks are primarily associated with the common functional groups of clay minerals, including OH deformations and the bending vibrations of Si and Al networks (Table 1). Much of the decrease in absorbance can be attributed to the decomposition of the clay mineral structures resulting from dehydroxylation, which occurs at temperatures between 100 to 500°C and between 100 to 650°C for kaolinite and both illite and Fe-smectite, respectively (Murad & Wagner, 1998; Smykatz-Kloss et al., 2003; Manoharan et al., 2011). The removal of OH from the clay mineral's

structure results in a significant decrease of the vibrations associated with the OH group, although some minerals, such as micas, only begin to dehydroxylize at temperatures above 700°C (Gaines & Vedder, 1964; Smykatz-Kloss et al., 2003).



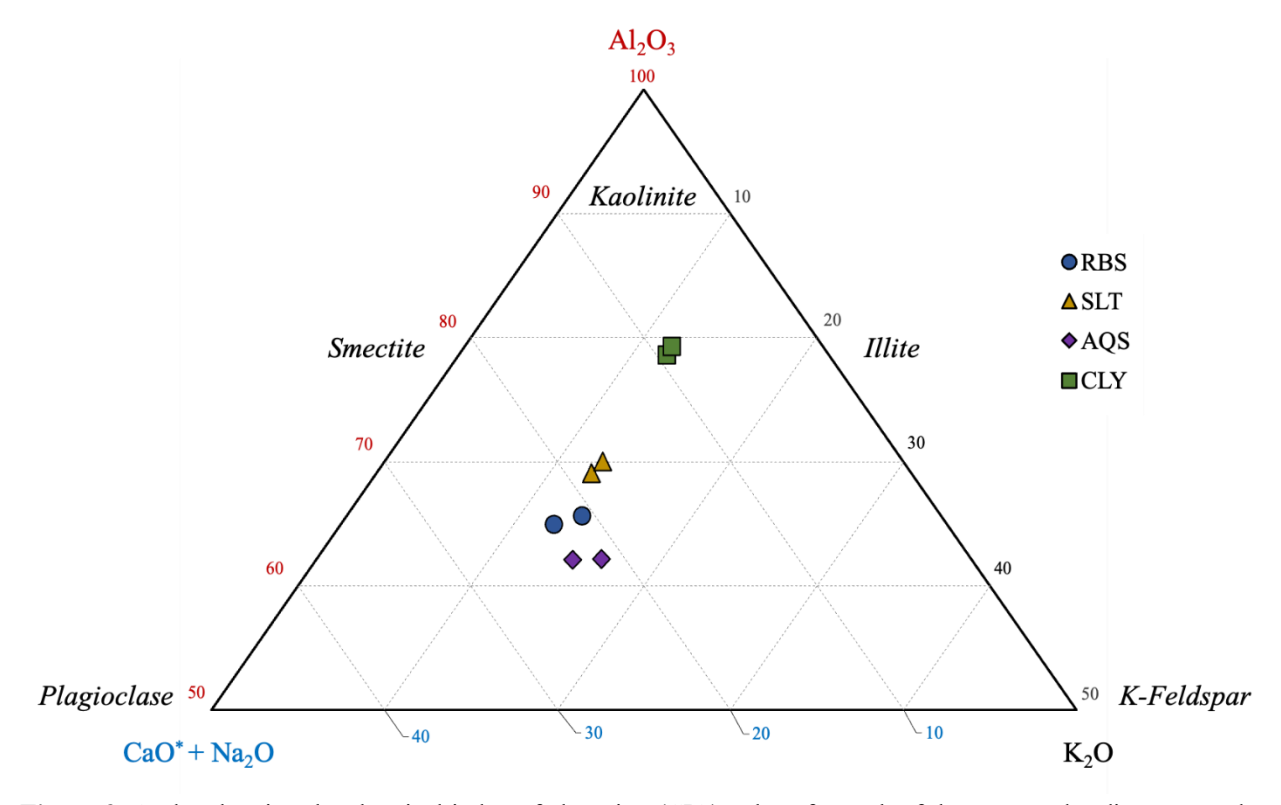


Figure 3. A plot showing the chemical index of alteration (CIA) values for each of the untreated sediment samples from each lithology along with the correlated mineral hosts displayed on the sides of the pyramid (Nesbitt & Young, 1982). The elemental concentrations used to calculate the CIA values are from the same sediment samples and were presented in Varner et al. (2022).

4.2 Fe mineralogy and transformations

The thermal treatment of sediments also serves as an indicator of the nature of Fe in the sample as both Fe-oxides and the structural Fe in clay minerals experience diagnostic transformations from increases in temperature. For example, the direct dehydroxylation of goethite and transformation to hematite species begins at 200-280°C (Murad & Wagner, 1998; Pomiès et al., 1999; Ruan et al., 2002; de Faria & Lopes, 2007; Liu et al., 2013b), whereas for Fe associated in

the structure of clay minerals, this transformation must be preceded by the structural deformation and collapse of the mineral lattice above 400°C (Lugassi et al., 2014). The oxidation of structural Fe(II) is accelerated by thermal treatment (Zhang et al., 2023), the Fe which can no longer be accommodated in the thermally altered silicate structures will then proceed to form hematite as the temperature increases (Murad & Wagner, 1996; Murad & Wagner, 1998; Murad et al., 2002; Araújo et al., 2004). Murad and Wagner (1998) found that divalent Fe was absent in illite above temperatures of 300°C whereas Fe(III) increased from 350 to 450°C, causing a change in color to a deeper reddish-brown hue. A similar process is likely the cause for the dramatic increase in the reddish-brown hues of the thermally treated SLT and CLY samples.

Although the vibrational frequencies of clay minerals may obscure the diagnostic bands of Fe-oxides, the previous application of FTIR for Fe-oxide phase transformation suggests that absorbance bands are a good indicator of the migration of excess hydroxyl units from goethite to hematite (Ruan et al., 2001). In the FTIR spectra, the peaks that are typically diagnostic of hydroxyl deformations in goethite (δ-OH deformation at 900 cm⁻¹ and γ-OH deformation at 795 cm⁻¹) were observed to decrease in all samples following thermal treatment (Fig. 1) (Prasad et al., 2006; Liu et al., 2013a). Furthermore, the decrease of the shoulder at 916 cm⁻¹ and the broadening and decrease in the absorbance band at 534 cm⁻¹ in the FTIR spectra of the treated samples is indicative of the dehydroxylation of goethite and of the OH substitution for O in the Fe-O bond of goethite and hydrohematite, respectively (Ruan et al., 2002; Chen et al., 2021). The removal of OH from the goethite structure as the temperature increases causes the band centered at 534 cm⁻¹ to shift to lower wavelengths and broaden. The broadening of this peak is observed in the thermally treated samples from ~600 to 452 cm⁻¹, is consistent with previous work using FTIR techniques to

investigate the thermal transformation of both natural goethite and Al-substituted goethite to hematite (Walter et al., 2001; Ruan et al., 2002; Prasad et al., 2006).

345

346

347

348

349

350

351

352

353

354

355

356

357

358

359

360

361

362

363

364

365

366

367

The application of DR spectroscopy in the 400 to 700 nm range is sensitive to minute amounts of Fe in the samples and can be used to differentiate between Fe(II) and Fe(III) in the samples (Horneman et al., 2004). In the untreated sediment, Fe(III) was present in the RBS and AOS and was not observed readily in either the SLT or CLY sediment. However, the thermally treated sediments showed an increase in the Fe(III) of all samples as indicated by the increase of the DR slope (Fig. 2a). The ΔR spectra of the untreated samples showed the presence of Fe(III) as goethite in the sand samples (peaks at 420 and 500 nm) and little to no Fe(III) in the sand samples. However, following thermal treatment, the presence of hematite (~560 nm) was observed in all samples (Fig. 2b) (Horneman et al., 2004; Wu et al., 2016; Cao et al., 2022). Interestingly, the hematite peak in the sand samples was located at 560 nm whereas the hematite peak in the thermally treated SLT and CLY samples was shifted down to 550 nm and exhibited a lower reflectance value despite higher initial bulk Fe concentrations. The shift of the hematite peak may be indicative of the initial Fe mineralogy of the samples. The sands experienced the direct transformation of goethite to hematite, whereas the Fe in the SLT and CLY was incorporated as structural Fe(II) which was only transformed to hematite following the structural deformation of clay minerals (Fig. 2b). These proposed mechanisms of hematite formation are supported by the increase of the ΔR value at 520 nm after thermal treatment, which show minimal changes for the sand samples (0.02) compared to that of the silt (0.48) and clay (0.68), indicating a greater increase in the proportion of Fe(III) in SLT and CLY (Horneman et al., 2004). The proportion of hematite relative to goethite should increase with increasing temperature, however, in the case of the SLT and CLY samples where the Fe was mostly present in the structure of clay minerals, the hematite was produced indirectly from

the degradation of clay minerals. Here we show that the thermal treatment of sediments, combined with DR and FTIR spectroscopy, is useful in its application to determine the relative proportions of Fe in clay minerals as opposed to oxide coatings in sediment. The sand samples contained Fe as Fe-oxides/hydroxides coating sediment grains whereas the Fe of the finer grained SLT and CLY samples contained as structural Fe in clay minerals.

4.3 Mineral associations of As in the sediment

The initial concentrations of As in RBS, SLT, AQS, and CLY (6.0, 2.3, <1.3, 11.4 mg/kg, respectively) decreased after thermal treatment by an average of 1.4, 2.3, 1.1, and 6.3 mg/kg, respectively (Table 2). Removal of As during heating could be attributed to the volatilization of As. The volatilization of As is more intense under rapid combustion than under slow heating conditions (Wang & Tomita, 2003), and multiple studies investigating coal combustion note that As volatilization increases with temperature with around 80% of As being volatilized at temperatures of ~900°C (Senior et al., 2000; Wang & Tomita, 2003; Guo et al., 2004; Liu et al., 2016; Cheng et al., 2019). At temperatures less than 600°C, organic-bound arsenic is readily volatized (Liu et al., 2016), and any exchangeable As and As bound to poorly crystallized Fe-Mn (hydr)oxides are volatized at temperatures lower than 1000°C (Wang & Tomita, 2003; Wang et al., 2018). In pure clay samples (kaolin), Gray et al. (2001) found that between 22 and 40 % of As was volatized at temperatures of 520 to 1120°C. The removal of higher amounts of As from thermal treatment in the SLT and CLY samples suggests that a larger portion of the As in these sediments is associated with OM, specifically in CLY.

The association of As with organic-rich clays has been well documented in the Bengal basin (Anawar et al., 2002; Smedley & Kinniburgh, 2002; McArthur et al., 2004; Nath et al., 2009); similarly, the clay at the study site has been shown to be enriched in recalcitrant organic matter

with functional groups favoring the formation of As and ternary As-Fe-OM complexes (Varner et al., 2023, In Preparation). Within the Bengal basin, fine-grained deposits are dominated by the cooccurrence of OM, clay minerals, and amorphous oxide minerals, which provide an abundance of sorption sites to promote the adsorption and accumulation of As (Anawar et al., 2003). Furthermore, the incorporation of Fe in the mineral structure of clay minerals contributes to the elevated concentrations of Fe in the clay layers of the Bengal basin, as structural Fe(II) accounts for more than 50% of the mass of Fe in the subsurface (Zhang et al., 2023). The occurrence of reduced Fe in SLT and CLY is reflected by the correlations between both grain size and CIA with the difference of the ΔR at 520 nm caused by thermal treatment, which transforms structural Fe(II) to hematite phases at elevated temperatures (Fig. 4a, 4b) (Varner et al., 2022). Following the thermal decomposition of OM and clay minerals, it is likely that any associated As was liberated and subsequently volatilized during thermal treatment, whereas the structural Fe was transformed to hematite phases. An indication of this process is shown by the high correlation between the initial As concentrations and the difference in the ΔR at 520 nm of the samples before and after thermal treatment, which is a proxy for the amount of Fe(II) incorporated within the structure of clay minerals that is able to be transformed to hematite (Fig. 4c).

391

392

393

394

395

396

397

398

399

400

401

402

403

404

405

406

407

408

409

410

411

412

413

The coexistence of elevated Fe-hydroxides and OM along with As is a result of the affinity of Fe for both As and OM. However, the presence of phyllosilicates, such as kaolinite and illite, are known to incorporate or adsorb As (Charlet et al., 2007; Huyen et al., 2019). The thermal treatment of the sediments and resulting loss of As suggests that large portions of solid-phase As are associated with clay minerals or OM. While the release of As under environmental conditions in the aquifers of Bangladesh may be regulated by Fe-oxide reduction, OM and phyllosilicate clay minerals may directly regulate the mobility of much of the As in the solid-phase. The associations

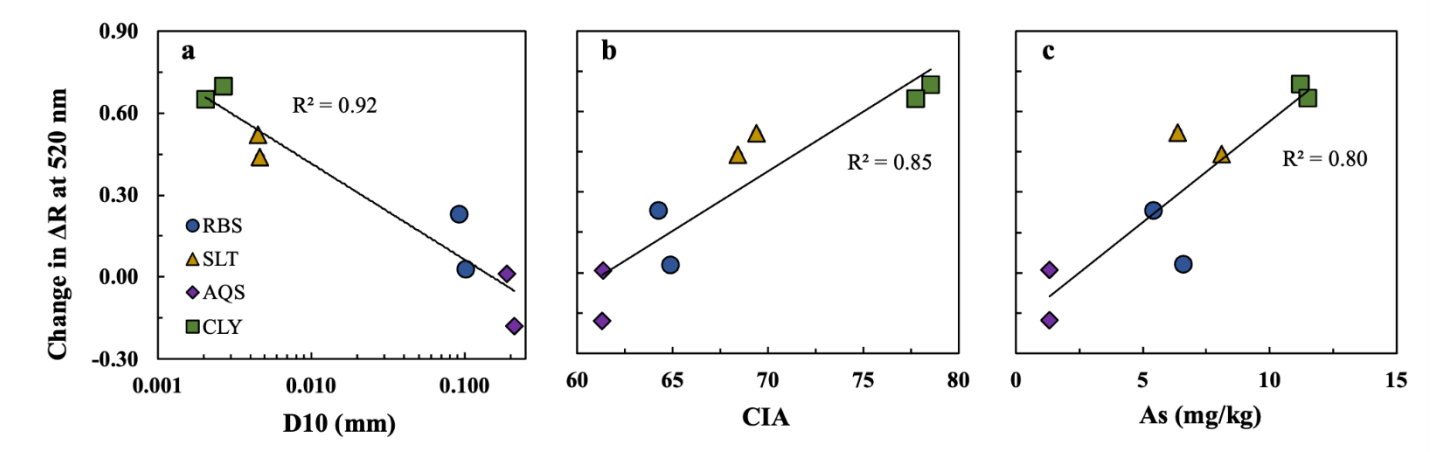


Figure 4. Correlation between the difference of the ΔR at 520 nm in the untreated and thermally treated sediment for each measured sample and (a) the D10 grain size; (b) the CIA value; and (c) the sedimentary concentration of As in the untreated samples. The difference of the ΔR at 520 nm serves as a proxy of the structural Fe in the sample that can be transformed to hematite phases at elevated temperatures. The D10 grain size and elemental concentrations for the CIA are presented in Varner et al. (2022).

of As with fine-grained sediments is clear, nevertheless, the understanding of As in deltaic aquifers would be benefited from further investigation into the role that various clay minerals and organic functional groups may have on the attenuation of As.

5 Conclusion

The combination of spectroscopic techniques along with thermal treatment has consistently been utilized for analysis of clay and Fe mineralogy in sediment and soil samples. Despite the known association of solid-phase As with both clay minerals and Fe-oxides in deltaic aquifers, the determination of the sedimentary associations of As in aquifer sediments from Bangladesh using the combined techniques has never been implemented, to our knowledge. This study employed the use of FTIR and diffuse reflectance techniques to define the mineralogical response of thermal treatments on riverbank and aquifer sediment from a contaminated aquifer along the Meghna River in Bangladesh.

Thermal treatment of all samples changed the sediment color to a more reddish-brown hue, with the greatest change in color exhibited by the silt and clay samples. The FTIR results of the

untreated and thermally treated sediment samples revealed the predominance of phyllosilicate clay minerals, primarily as illite, smectite, and kaolinite, which related to the As content of the sediment. Diffuse reflectance measurements showed that the Fe in the sand samples was present as goethite coatings, whereas Fe in the fine-grained silt and clay samples was largely present as reduced Fe within the structure of clay minerals. Initial As concentrations were higher in the clay and silt samples (11.4, 7.3, mg/kg, respectively) than the riverbank and aquifer sand samples (6.0, <1.3 mg/kg, respectively). Following thermal treatment, more As was volatilized in the clay and silt samples with the concentrations of As in the clay, silt, riverbank sand, and aquifer sand decreasing by 52, 29, 23, and 17 %, respectively. The highly reactive structural Fe(II) in the silt and clay samples may explain the high levels of association documented between Fe, OM, and As within the shallow aquifers of Bangladesh. These results advance our understanding of the distribution of As within the aquifers of Bangladesh. Whereas the mobilization of As may be explained by the reductive dissolution of Fe-oxides, these findings imply that clay minerals and OM may strongly regulate the mobility and fate of solid-phase As.

6 Acknowledgements

We acknowledge assistance received from the students at the University of Dhaka for assistance in the field. We would like to thank the UTSA Chemistry Department for providing access to the FTIR instrument and to Department of Geology and Geophysics at Texas A&M University for access to the XRF. Funding was provided to Peter S. Knappett, M. Bayani Cardenas, and Saugata Datta by the National Science Foundation Hydrologic Sciences grant numbers EAR- 1852652, EAR- 1852653, and EAR- 1940772, respectively.

7 Credit author statement

Thomas Varner: Conceptualization, Methodology, Validation, Formal analysis, Investigation, Data curation, Writing original draft, Visualization. Harshad V. Kulkarni: Conceptualization, Methodology, Validation, Formal analysis, Investigation, Data curation, Writing – review & editing, Visualization, Supervision. Peter Knappett: Resources, Writing – review and editing, Project administration, Funding acquisition. M. Bayani Cardenas: Resources, Writing – review and editing, Project administration, Funding acquisition. Saugata Datta: Conceptualization, Resources, Writing – review and editing, Project administration, Supervision, Funding acquisition.

- 458 Allison, M. A., Khan, S., Goodbred Jr, S. L., & Kuehl, S. A. (2003). Stratigraphic evolution of the late 459 Holocene Ganges–Brahmaputra lower delta plain. *Sedimentary Geology*, *155*(3-4), 317-342.
- Anawar, H., Komaki, K., Akai, J., Takada, J., Ishizuka, T., Takahashi, T., Yoshioka, T., & Kato, K. (2002).

 Diagenetic control on arsenic partitioning in sediments of the Meghna River delta, Bangladesh.

 Environmental Geology, 41(7), 816-825.
- Anawar, H. M., Akai, J., Komaki, K., Terao, H., Yoshioka, T., Ishizuka, T., Safiullah, S., & Kato, K. (2003).

 Geochemical occurrence of arsenic in groundwater of Bangladesh: sources and mobilization processes. *Journal of Geochemical Exploration*, 77(2-3), 109-131.
- Araújo, J. H. d., Silva, N. F. d., Acchar, W., & Gomes, U. U. (2004). Thermal decomposition of illite. *Materials Research*, *7*, 359-361.
 - Arimoto, R., Balsam, W., & Schloesslin, C. (2002). Visible spectroscopy of aerosol particles collected on filters: iron-oxide minerals. *Atmospheric Environment*, *36*(1), 89-96.
 - Ayers, J. C., Patton, B., & Dietrich, M. (2020). Preliminary Evidence of Transport-Limited Chemical Weathering and Element Immobility in the Ganges Tidal Delta Plain of Bangladesh. *Geochemistry, Geophysics, Geosystems*, 21(8), e2020GC009029.
 - Balsam, W. L., & Damuth, J. E. (2000). 31. FURTHER INVESTIGATIONS OF SHIPBOARD VS. SHORE-BASED SPECTRAL DATA: IMPLICATIONS FOR INTERPRETING LEG 164 SEDIMENT COMPOSITION1. Proceedings of the Ocean Drilling Program. Scientific results,
 - Beaulieu, B. T., & Savage, K. S. (2005). Arsenate adsorption structures on aluminum oxide and phyllosilicate mineral surfaces in smelter-impacted soils. *Environmental Science & Technology*, 39(10), 3571-3579.
 - Berube, M., Jewell, K., Myers, K. D., Knappett, P. S., Shuai, P., Hossain, A., Lipsi, M., Hossain, S., Aitkenhead-Peterson, J., & Ahmed, K. (2018). The fate of arsenic in groundwater discharged to the Meghna River, Bangladesh. *Environ. Chem.*, 15, 29.
 - BGS&DPHE. (2001). Arsenic contamination of groundwater in Bangladesh.
 - Bhattacharya, P., Jacks, G., Jana, J., Sracek, A., Gustafsson, J., & Chatterjee, D. (2001). Geochemistry of the Holocene alluvial sediments of Bengal Delta Plain from West Bengal, India: implications on arsenic contamination in groundwater. *Groundwater arsenic contamination in the Bengal Delta Plain of Bangladesh*, 3084, 21-40.
 - Cao, W., Jiang, Z., Gai, C., Barrón, V., Torrent, J., Zhong, Y., & Liu, Q. (2022). Re-Visiting the Quantification of Hematite by Diffuse Reflectance Spectroscopy. *Minerals*, *12*(7), 872.
 - Chakraborty, M., Mukherjee, A., & Ahmed, K. M. (2015). A review of groundwater arsenic in the Bengal Basin, Bangladesh and India: from source to sink. *Current Pollution Reports*, 1(4), 220-247.
 - Charlet, L., Chakraborty, S., Appelo, C., Roman-Ross, G., Nath, B., Ansari, A., Lanson, M., Chatterjee, D., & Mallik, S. B. (2007). Chemodynamics of an arsenic "hotspot" in a West Bengal aquifer: a field and reactive transport modeling study. *Applied geochemistry*, 22(7), 1273-1292.
 - Chen, S. A., Heaney, P. J., Post, J. E., Fischer, T. B., Eng, P. J., & Stubbs, J. E. (2021). Superhydrous hematite and goethite: A potential water reservoir in the red dust of Mars? *Geology*, *49*(11), 1343-1347.
 - Cheng, R., Zhang, H., & Ni, H. (2019). Arsenic removal from arsenopyrite-bearing iron ore and arsenic recovery from dust ash by roasting method. *Processes*, 7(10), 754.
- Datta, S., Mailloux, B., Jung, H.-B., Hoque, M., Stute, M., Ahmed, K., & Zheng, Y. (2009). Redox trapping of arsenic during groundwater discharge in sediments from the Meghna riverbank in Bangladesh.

 Proceedings of the National Academy of Sciences, 106(40), 16930-16935.
- de Faria, D. L. A., & Lopes, F. N. (2007). Heated goethite and natural hematite: can Raman spectroscopy be used to differentiate them? *Vibrational spectroscopy*, *45*(2), 117-121.

- 503 Deng, Y., & Dixon, J. B. (2002). Soil organic matter and organic-mineral interactions. *Soil mineralogy with* 604 *environmental applications*, *7*, 69-107.
- Edwards, H., Drummond, L., & Russ, J. (1998). Fourier-transform Raman spectroscopic study of pigments in native American Indian rock art: Seminole Canyon. *Spectrochimica Acta Part A: Molecular and Biomolecular Spectroscopy*, *54*(12), 1849-1856.
- Farmer, V. (1974a). The anhydrous oxide minerals.
- 509 Farmer, V. (1974b). The layer silicates.

525

526 527

528

529

530

531

532

533

534

535

- Flanagan, S. V., Johnston, R. B., & Zheng, Y. (2012). Arsenic in tube well water in Bangladesh: health and economic impacts and implications for arsenic mitigation. *Bulletin of the World Health Organization*, *90*, 839-846.
- Frost, R. L., Kloprogge, J. T., Russell, S. C., & Szetu, J. L. (1999). Vibrational spectroscopy and dehydroxylation of aluminum (oxo) hydroxides: gibbsite. *Applied spectroscopy*, *53*(4), 423-434.
- Frost, R. L., Ruan, H., Kloprogge, J. T., & Gates, W. P. (2000). Dehydration and dehydroxylation of nontronites and ferruginous smectite. *Thermochimica Acta*, *346*(1-2), 63-72.
- 517 Gaines, G., & Vedder, W. (1964). Dehydroxylation of muscovite. *Nature*, 201(4918), 495-495.
- Glodowska, M., Stopelli, E., Schneider, M., Lightfoot, A., Rathi, B., Straub, D., Patzner, M., Duyen, V.,
 Members, A. T., & Berg, M. (2020). Role of in situ natural organic matter in mobilizing As during
 microbial reduction of FeIII-mineral-bearing aquifer sediments from Hanoi (Vietnam).

 Environmental Science & Technology, 54(7), 4149-4159.
- Goldberg, S. (2002). Competitive adsorption of arsenate and arsenite on oxides and clay minerals. *Soil Science Society of America Journal*, *66*(2), 413-421.
 - Gray, D. B., Watts, F., & Overcamp, T. J. (2001). Volatility of arsenic in contaminated clay at high temperatures. *Environmental engineering science*, 18(1), 1-7.
 - Guo, R., Yang, J., & Liu, Z. (2004). Thermal and chemical stabilities of arsenic in three Chinese coals. *Fuel processing technology*, 85(8-10), 903-912.
 - Hasan, M. A., Ahmed, K. M., Sracek, O., Bhattacharya, P., Von Broemssen, M., Broms, S., Fogelström, J., Mazumder, M. L., & Jacks, G. (2007). Arsenic in shallow groundwater of Bangladesh: investigations from three different physiographic settings. *Hydrogeology Journal*, 15(8), 1507-1522.
 - Hofstetter, T. B., Schwarzenbach, R. P., & Haderlein, S. B. (2003). Reactivity of Fe (II) species associated with clay minerals. *Environmental Science & Technology*, *37*(3), 519-528.
 - Horneman, A., van Geen, A., Kent, D. V., Mathe, P., Zheng, Y., Dhar, R., O'connell, S., Hoque, M., Aziz, Z., & Shamsudduha, M. (2004). Decoupling of As and Fe release to Bangladesh groundwater under reducing conditions. Part I: Evidence from sediment profiles. *Geochimica et Cosmochimica Acta, 68*(17), 3459-3473.
- Huang, J., Jones, A., Waite, T. D., Chen, Y., Huang, X., Rosso, K. M., Kappler, A., Mansor, M., Tratnyek, P. G., & Zhang, H. (2021). Fe (II) redox chemistry in the environment. *Chemical Reviews*, *121*(13), 8161-8233.
- Huyen, D. T., Tabelin, C. B., Thuan, H. M., Dang, D. H., Truong, P. T., Vongphuthone, B., Kobayashi, M., & Igarashi, T. (2019). The solid-phase partitioning of arsenic in unconsolidated sediments of the Mekong Delta, Vietnam and its modes of release under various conditions. *Chemosphere*, *233*, 512-523.
- Islam, F. S., Gault, A. G., Boothman, C., Polya, D. A., Charnock, J. M., Chatterjee, D., & Lloyd, J. R. (2004).
 Role of metal-reducing bacteria in arsenic release from Bengal delta sediments. *Nature*,
 430(6995), 68-71.
- Jordán, M., Sanfeliu, T., & De la Fuente, C. (2001). Firing transformations of Tertiary clays used in the manufacturing of ceramic tile bodies. *Applied clay science*, *20*(1-2), 87-95.

- Jung, H. B., Bostick, B. C., & Zheng, Y. (2012). Field, experimental, and modeling study of arsenic partitioning across a redox transition in a Bangladesh aquifer. *Environ Sci Technol*, 46(3), 1388-1395. https://doi.org/10.1021/es2032967
- Jung, H. B., Zheng, Y., Rahman, M. W., Rahman, M. M., & Ahmed, K. M. (2015). Redox Zonation and Oscillation in the Hyporheic Zone of the Ganges-Brahmaputra-Meghna Delta: Implications for the Fate of Groundwater Arsenic during Discharge. *Appl Geochem*, *63*, 647-660. https://doi.org/10.1016/j.apgeochem.2015.09.001

- Khan, M. H. R., Liu, J., Liu, S., Seddique, A. A., Cao, L., & Rahman, A. (2019). Clay mineral compositions in surface sediments of the Ganges-Brahmaputra-Meghna river system of Bengal Basin, Bangladesh. *Marine Geology*, 412, 27-36.
- Komadel, P., Lear, P. R., & Stucki, J. W. (1990). Reduction and reoxidation of nontronite: Extent of reduction and reaction rates. *Clays and Clay Minerals*, *38*, 203-208.
- Komadel, P., Madejová, J., & Stucki, J. W. (2006). Structural Fe (III) reduction in smectites. *Applied clay science*, *34*(1-4), 88-94.
 - Liu, G., Fernandez, A., & Cai, Y. (2011). Complexation of arsenite with humic acid in the presence of ferric iron. *Environmental Science & Technology*, 45(8), 3210-3216.
 - Liu, H., Chen, T., Qing, C., Xie, Q., & Frost, R. L. (2013a). Confirmation of the assignment of vibrations of goethite: An ATR and IES study of goethite structure. *Spectrochimica Acta Part A: Molecular and Biomolecular Spectroscopy*, *116*, 154-159.
 - Liu, H., Chen, T., Zou, X., Qing, C., & Frost, R. L. (2013b). Thermal treatment of natural goethite: Thermal transformation and physical properties. *Thermochimica Acta*, *568*, 115-121.
 - Liu, H., Pan, W.-P., Wang, C., & Zhang, Y. (2016). Volatilization of arsenic during coal combustion based on isothermal thermogravimetric analysis at 600–1500° C. *Energy & fuels*, *30*(8), 6790-6798.
 - Lowers, H. A., Breit, G. N., Foster, A. L., Whitney, J., Yount, J., Uddin, M. N., & Muneem, A. A. (2007). Arsenic incorporation into authigenic pyrite, Bengal Basin sediment, Bangladesh. *Geochimica et Cosmochimica Acta*, 71(11), 2699-2717.
 - Lugassi, R., Ben-Dor, E., & Eshel, G. (2014). Reflectance spectroscopy of soils post-heating—Assessing thermal alterations in soil minerals. *Geoderma*, *213*, 268-279.
 - Madejová, J., Gates, W., & Petit, S. (2017). IR spectra of clay minerals. In *Developments in clay science* (Vol. 8, pp. 107-149). Elsevier.
 - Manoharan, C., Sutharsan, P., Dhanapandian, S., Venkatachalapathy, R., & Asanulla, R. M. (2011). Analysis of temperature effect on ceramic brick production from alluvial deposits, Tamilnadu, India. *Applied clay science*, *54*(1), 20-25.
 - Margenot, A. J., Calderón, F. J., Goyne, K. W., Dmukome, F. N., & Parikh, S. (2016). IR spectroscopy, soil analysis applications. In *Encyclopedia of spectroscopy and spectrometry* (pp. 448-454). Elsevier.
 - Masuda, H., Shinoda, K., Okudaira, T., Takahashi, Y., & Noguchi, N. (2012). Chlorite—source of arsenic groundwater pollution in the Holocene aquifer of Bangladesh. *Geochemical Journal*, 46(5), 381-391.
 - McArthur, J., Banerjee, D., Hudson-Edwards, K., Mishra, R., Purohit, R., Ravenscroft, P., Cronin, A., Howarth, R., Chatterjee, A., & Talukder, T. (2004). Natural organic matter in sedimentary basins and its relation to arsenic in anoxic ground water: the example of West Bengal and its worldwide implications. *Applied geochemistry*, *19*(8), 1255-1293.
 - McArthur, J., Ravenscroft, P., Safiulla, S., & Thirlwall, M. (2001). Arsenic in groundwater: testing pollution mechanisms for sedimentary aquifers in Bangladesh. *Water Resources Research*, 37(1), 109-117.
- Mihajlov, I., Mozumder, M. R. H., Bostick, B. C., Stute, M., Mailloux, B. J., Knappett, P. S., Choudhury, I., Ahmed, K. M., Schlosser, P., & van Geen, A. (2020). Arsenic contamination of Bangladesh aquifers exacerbated by clay layers. *Nature communications*, *11*(1), 1-9.

- Morris, R. V., Lauer Jr, H. V., Lawson, C. A., Gibson Jr, E. K., Nace, G. A., & Stewart, C. (1985). Spectral and other physicochemical properties of submicron powders of hematite (α-Fe2O3), maghemite (γ-Fe2O3), magnetite (Fe3O4), goethite (α-FeOOH), and lepidocrocite (γ-FeOOH). *Journal of Geophysical Research: Solid Earth, 90*(B4), 3126-3144.
- Mukherjee, A., Verma, S., Gupta, S., Henke, K. R., & Bhattacharya, P. (2014). Influence of tectonics, sedimentation and aqueous flow cycles on the origin of global groundwater arsenic: paradigms from three continents. *Journal of Hydrology*, *518*, 284-299.
- Murad, E., & Wagner, U. (1996). The thermal behaviour of an Fe-rich illite. Clay Minerals, 31(1), 45-52.
- Murad, E., & Wagner, U. (1998). Clays and clay minerals: the firing process. *Hyperfine interactions*, *117*(1), 337-356.
- Murad, E., Wagner, U., Wagner, F., & Häusler, W. (2002). The thermal reactions of montmorillonite: a Mössbauer study. *Clay Minerals*, *37*(4), 583-590.

609

610

613

614

615

616

617

618

623

624

625

626

627

628

629

- Nath, B., Chakraborty, S., Burnol, A., Stüben, D., Chatterjee, D., & Charlet, L. (2009). Mobility of arsenic in the sub-surface environment: An integrated hydrogeochemical study and sorption model of the sandy aquifer materials. *Journal of Hydrology*, 364(3-4), 236-248.
- Nesbitt, H., & Young, G. (1982). Early Proterozoic climates and plate motions inferred from major element chemistry of lutites. *Nature*, *299*(5885), 715-717.
 - Neumann, A., Hofstetter, T. B., Lüssi, M., Cirpka, O. A., Petit, S., & Schwarzenbach, R. P. (2008). Assessing the redox reactivity of structural iron in smectites using nitroaromatic compounds as kinetic probes. *Environmental Science & Technology*, 42(22), 8381-8387.
 - Neumann, A., Hofstetter, T. B., Skarpeli-Liati, M., & Schwarzenbach, R. P. (2009). Reduction of polychlorinated ethanes and carbon tetrachloride by structural Fe (II) in smectites. *Environmental Science & Technology*, *43*(11), 4082-4089.
- Nickson, R., McArthur, J., Burgess, W., Ahmed, K. M., Ravenscroft, P., & Rahmanñ, M. (1998). Arsenic poisoning of Bangladesh groundwater. *Nature*, *395*(6700), 338-338.
- Nickson, R., McArthur, J., Ravenscroft, P., Burgess, W., & Ahmed, K. (2000). Mechanism of arsenic release to groundwater, Bangladesh and West Bengal. *Applied geochemistry*, *15*(4), 403-413.
 - Parikh, S. J., Goyne, K. W., Margenot, A. J., Mukome, F. N., & Calderón, F. J. (2014). Soil chemical insights provided through vibrational spectroscopy. *Advances in agronomy*, *126*, 1-148.
 - Polizzotto, M. L., Harvey, C. F., Li, G., Badruzzman, B., Ali, A., Newville, M., Sutton, S., & Fendorf, S. (2006). Solid-phases and desorption processes of arsenic within Bangladesh sediments. *Chemical Geology*, 228(1-3), 97-111.
 - Polizzotto, M. L., Harvey, C. F., Sutton, S. R., & Fendorf, S. (2005). Processes conducive to the release and transport of arsenic into aquifers of Bangladesh. *Proceedings of the National Academy of Sciences*, 102(52), 18819-18823.
- Pomiès, M. P., Menu, M., & Vignaud, C. (1999). Red palaeolithic pigments: natural hematite or heated goethite? *Archaeometry*, *41*(2), 275-285.
- 633 Prasad, P., Prasad, K. S., Chaitanya, V. K., Babu, E., Sreedhar, B., & Murthy, S. R. (2006). In situ FTIR study 634 on the dehydration of natural goethite. *Journal of Asian Earth Sciences*, *27*(4), 503-511.
- 635 Qiao, W., Guo, H., He, C., Shi, Q., Xiu, W., & Zhao, B. (2020). Molecular evidence of arsenic mobility linked 636 to biodegradable organic matter. *Environmental Science & Technology*, *54*(12), 7280-7290.
- Redman, A. D., Macalady, D. L., & Ahmann, D. (2002). Natural organic matter affects arsenic speciation and sorption onto hematite. *Environmental Science & Technology*, *36*(13), 2889-2896.
- Ruan, H., Frost, R., Kloprogge, J., & Duong, L. (2002). Infrared spectroscopy of goethite dehydroxylation:
 III. FT-IR microscopy of in situ study of the thermal transformation of goethite to hematite.

 Spectrochimica Acta Part A: Molecular and Biomolecular Spectroscopy, 58(5), 967-981.

- Ruan, H., Frost, R., & Kloprogge, J. T. (2001). The behavior of hydroxyl units of synthetic goethite and its dehydroxylated product hematite. *Spectrochimica Acta Part A: Molecular and Biomolecular Spectroscopy*, *57*(13), 2575-2586.
- Russell, J., & Fraser, A. (1994). Infrared methods. *Clay Mineralogy: Spectroscopic and chemical determinative methods*, 11-67.

- Seddique, A. A., Masuda, H., Mitamura, M., Shinoda, K., Yamanaka, T., Itai, T., Maruoka, T., Uesugi, K., Ahmed, K. M., & Biswas, D. K. (2008). Arsenic release from biotite into a Holocene groundwater aquifer in Bangladesh. *Applied geochemistry*, 23(8), 2236-2248.
 - Senior, C. L., Bool III, L. E., & Morency, J. R. (2000). Laboratory study of trace element vaporization from combustion of pulverized coal. *Fuel processing technology*, *63*(2-3), 109-124.
- Sharma, P., Ofner, J., & Kappler, A. (2010). Formation of binary and ternary colloids and dissolved complexes of organic matter, Fe and As. *Environmental Science & Technology*, 44(12), 4479-4485.
- Shuai, P., Knappett, P. S., Hossain, S., Hosain, A., Rhodes, K., Ahmed, K. M., & Cardenas, M. B. (2017). The impact of the degree of aquifer confinement and anisotropy on tidal pulse propagation. *Groundwater*, *55*(4), 519-531.
- Smedley, P. L., & Kinniburgh, D. G. (2002). A review of the source, behaviour and distribution of arsenic in natural waters. *Applied geochemistry*, *17*(5), 517-568.
- Smith, A. H., Lingas, E. O., & Rahman, M. (2000). Contamination of drinking-water by arsenic in Bangladesh: a public health emergency. *Bulletin of the World Health Organization*, 78, 1093-1103.
- Smykatz-Kloss, W., Heide, K., & Klinke, W. (2003). Applications of thermal methods in the geosciences. In *Handbook of thermal analysis and calorimetry* (Vol. 2, pp. 451-593). Elsevier.
- Strens, R., & Wood, B. (1979). Diffuse reflectance spectra and optical properties of some iron and titanium oxides and oxyhydroxides. *Mineralogical Magazine*, *43*(327), 347-354.
- Stucki, J. (2006). Properties and behaviour of iron in clay minerals. *Developments in clay science*, *1*, 423-475.
- Stucki, J. W. (2011). A review of the effects of iron redox cycles on smectite properties. *Comptes Rendus Geoscience*, *343*(2-3), 199-209.
- Tabelin, C. B., Sasaki, R., Igarashi, T., Park, I., Tamoto, S., Arima, T., Ito, M., & Hiroyoshi, N. (2017). Simultaneous leaching of arsenite, arsenate, selenite and selenate, and their migration in tunnel-excavated sedimentary rocks: II. Kinetic and reactive transport modeling. *Chemosphere*, 188, 444-454.
- Torrent, J., & Barrón, V. (2002). Diffuse reflectance spectroscopy of iron oxides. *Encyclopedia of surface and Colloid Science*, *1*, 1438-1446.
- van Geen, A., Ahmed, E. B., Pitcher, L., Mey, J. L., Ahsan, H., Graziano, J. H., & Ahmed, K. M. (2014). Comparison of two blanket surveys of arsenic in tubewells conducted 12 years apart in a 25 km(2) area of Bangladesh. *Sci Total Environ*, 488-489, 484-492. https://doi.org/10.1016/j.scitotenv.2013.12.049
- van Geen, A., Zheng, Y., Versteeg, R., Stute, M., Horneman, A., Dhar, R., Steckler, M., Gelman, A., Small, C., Ahsan, H., Graziano, J. H., Hussain, I., & Ahmed, K. M. (2003). Spatial variability of arsenic in 6000 tube wells in a 25 km2area of Bangladesh. *Water Resources Research*, 39(5). https://doi.org/10.1029/2002wr001617
- Varner, T. S., Kulkarni, H. V., Nguyen, W., Kwak, K., Cardenas, M. B., Knappett, P. S., Ojeda, A. S., Malina, N., Bhuiyan, M. U., & Ahmed, K. M. (2022). Contribution of sedimentary organic matter to arsenic mobilization along a potential natural reactive barrier (NRB) near a river: The Meghna river, Bangladesh. *Chemosphere*, 308, 136289.
- Vega, M. A., Kulkarni, H. V., Johannesson, K. H., Taylor, R. J., & Datta, S. (2020). Mobilization of cooccurring trace elements (CTEs) in arsenic contaminated aquifers in the Bengal basin. *Applied* geochemistry, 122, 104709.

- Walter, D., Buxbaum, G., & Laqua, W. (2001). The mechanism of the thermal transformation from goethite to hematite. *Journal of Thermal Analysis and Calorimetry*, *63*(3), 733-748.
- Wang, C., Liu, H., Zhang, Y., Zou, C., & Anthony, E. J. (2018). Review of arsenic behavior during coal combustion: volatilization, transformation, emission and removal technologies. *Progress in Energy and Combustion Science*, 68, 1-28.
- Wang, J., & Tomita, A. (2003). A chemistry on the volatility of some trace elements during coal combustion and pyrolysis. *Energy & fuels*, *17*(4), 954-960.

700 701

705

706

707

708

709

710

711

715

- Wang, S., & Mulligan, C. N. (2006). Natural attenuation processes for remediation of arsenic contaminated soils and groundwater. *Journal of Hazardous Materials*, *138*(3), 459-470.
 - Wu, G., Xu, T., Zhang, X., Zhang, C., & Yan, N. (2016). The visible spectroscopy of iron oxide minerals in dust particles from ice cores on the Tibetan Plateau. *Tellus B: Chemical and Physical Meteorology*, 68(1), 29191.
- Xue, Q., Ran, Y., Tan, Y., Peacock, C. L., & Du, H. (2019). Arsenite and arsenate binding to ferrihydrite
 organo-mineral coprecipitate: Implications for arsenic mobility and fate in natural environments.
 Chemosphere, 224, 103-110.
 - Zhang, F., Li, X., Duan, L., Zhang, H., Gu, W., Yang, X., Li, J., He, S., Yu, J., & Ren, M. (2021). Effect of different DOM components on arsenate complexation in natural water. *Environmental pollution*, *270*, 116221.
 - Zhang, W., Li, X., Shen, J., Sun, Z., Zhou, X., Li, F., Ma, F., & Gu, Q. (2023). Insights into the degradation process of phenol during in-situ thermal desorption: The overlooked oxidation of hydroxyl radicals from oxygenation of reduced Fe-bearing clay minerals. *Journal of Hazardous Materials*, 444, 130401.
- Zheng, Y., Stute, M., Van Geen, A., Gavrieli, I., Dhar, R., Simpson, H., Schlosser, P., & Ahmed, K. (2004).
 Redox control of arsenic mobilization in Bangladesh groundwater. *Applied geochemistry*, *19*(2),
 201-214.